VII International Conference on Computational Methods in Marine Engineering
MARINE 2017
M. Visonneau, P. Queutey and D. Le Touzé (Eds)

OPTIMIZED DBD PLASMA ACTUATOR SYSTEM FOR THE SUPPRESSION OF FLOW SEPARATION OVER A NACA0012 PROFILE

LAURA PASQUALE*, DANILO DURANTE†, MATTEO DIEZ† AND RICCARDO BROGLIA†

*Aerospace Technology Centre, Faculty of Engineering
University of Nottingham, UK
e-mail: Laura.Pasquale@nottingham.ac.uk - Web page: http://www.nottingha.ac.uk

†National Research Council-Marine Technology Research Institute (CNR-INSEAN)
Via di Vallerano 139, 00128 Rome, Italy
e-mail: danilo.durante@cnr.it matteo.diez@cnr.it riccardo.broglia@cnr.it - Web page: http://www.insean.cnr.it

Key words: Flow separation control, Robust control, Plasma actuators, Multi-objective deterministic particle swarm optimization

Abstract. We address the problem of controlling the unsteady flow separation over an aerofoil, using plasma actuators. Despite the complexity of the dynamics of interest, we show how the problem of controlling flow separation can be formulated as a simple output regulation problem, so that a simple control strategy may be used. Different configurations are tested, in order to identify optimal positions of the actuator/sensor pairs along the aerofoil, as well as the corresponding references for the available real-time velocity measurements. A multi-objective deterministic particle swarm optimization algorithm is applied to identify the set of non dominated configurations considering as objectives the time-averaged input signal and the drag-to-lift ratio. Accurate numerical simulations of incompressible flows around a NACA0012 profile at Reynolds $Re = 20,000$ and angle of attack 15° illustrate the effectiveness of the proposed approach, in the presence of complex nonlinear dynamics, which are neglected in the control design. Fast flow reattachment is achieved, along with both stabilisation and increase/reduction of the lift/drag, respectively. A major advantage of the presented method is that the chosen controlled outputs can be easily measured in realistic applications.

1 INTRODUCTION

Closed-loop flow control is aimed at altering a natural flow state into a more desirable state, which is chosen depending on control objectives. Crucial examples are: manipulation of flow separation, drag reduction, noise suppression, stall prevention *etc.* Within this context, the incorporation of control theory into many open problems in fluid mechanics presents a host

of new opportunities, with a wide range of applications in disparate fields (*e.g.* gas turbines, aircraft, as well as ground and marine vehicles). The control input is usually an electric signal, which has to be converted to a physical quantity by means of an actuator. A new and original technology using non-thermal surface plasmas has witnessed a significant growth in interest in recent years [see, for instance, 6, 14], as they: have no moving parts; exhibit an extremely fast time-response; are characterised by low mass and low input power. These surface dielectric barrier discharge (DBD) actuators are used to accelerate the near-wall flow, thus modifying the velocity profile within the boundary layer.

In this paper, we focus on the robust feedback control of the flow separation using plasma actuators. In most flow control applications the objective is to suppress the separation bubble, as it is responsible for both a loss of the lift and an increase of the drag and it might lead to stall conditions. Recent works on feedback flow separation control include [1], where a a slope-seeking algorithm is proposed to obtain maximum time-averaged lift. [4] proposed a retrospective cost adaptive algorithm to minimize the variation of the aerodynamic lift. However, the latter, which is the chosen output in both [1] and [4], cannot be measured in real-time in practical flow control applications.

Our objective is to solve the problem of directly controlling the unsteady flow separation using real-time velocity measurements, which are available in realistic applications [see, for instance, 16]. We propose this flow separation problem as a practical application of the new theoretical results in [11]. The aim of this paper is to show how, despite the high complexity of the system, a simple robust output regulator is sufficient to effectively suppress the flow separation along an aerofoil, using only one actuator/sensor pair. Accurate numerical simulations of flows past a NACA0012 profile are performed in order to test the control effectiveness, in the presence of complex nonlinear dynamics, which are neglected in the control design. A multi-objective deterministic particle swarm optimization (MODPSO) algorithm is finally applied to study the trade-off between the time-averaged input signal and the drag-to-lift ratio, varying the positions of the actuator/sensor pairs along the aerofoil, as well as the corresponding reference for the available real-time velocity measurements. Three sub-sets of non dominated configurations are identified and three solutions are selected accordingly for further investigations.

2 PROBLEM STATEMENT AND OBJECTIVES

This paper addresses the practical problem of robustly controlling the unsteady flow separation over an aerofoil, using the plasma actuator voltage as the control input and realistically available real-time velocity measurements as the control output. In particular, we aim to formulate and solve the flow separation problem, *i.e.*, to make

$$\partial_{\boldsymbol{n}} u_{\boldsymbol{\tau}}(t,\boldsymbol{x})|_{\Gamma_N} = \big(\boldsymbol{\tau}(\boldsymbol{x}) \cdot \nabla \boldsymbol{u}(t,\boldsymbol{x}) \cdot \boldsymbol{n}(\boldsymbol{x})\big)|_{\Gamma_N} > 0, \tag{1}$$

as a simple output regulation problem, *i.e.*, to make the measured output

$$\mathrm{y}(t) = u_\tau(t,\boldsymbol{x}_s) > \epsilon > 0. \tag{2}$$

Here: $\boldsymbol{u}$ is the time-dependent flow velocity vector; $\boldsymbol{x}$ and $\boldsymbol{x}_s$ denote the spatial coordinates and the sensor location, respectively; Γ_N represents the aerofoil boundary; $\boldsymbol{n}$ and $\boldsymbol{\tau}$ are the normal and tangent unit vectors to Γ_N, respectively.

Our objective is to design a robust output feedback control, along with a suitable reference signal y^* for y, in order to suppress the flow separation along the aerofoil in unknown scenarios, depending on uncertain parameters, *i.e.*, Reynolds number Re and angle of attack β. To this end, we assume there exist suitable configurations of actuators and sensors, along with suitable references ε for the output $\mathrm{y}(t)$, which guarantee that, given a certain range for both Re and β, the solution of the output regulation problem (2) implies the solution of the flow separation problem (1). This is formalised by the following assumption.

Assumption 1. *For any $\delta \geq 0$ there exist some references $\varepsilon > 0$, a $T_\varepsilon > 0$ and a $T_\delta \geq T_\varepsilon$ such that, if $y(t) > \varepsilon$ for all $t > T_\varepsilon$, then $\partial_{\boldsymbol{n}} u_{\boldsymbol{\tau}}(t, \boldsymbol{x})|_{\Gamma_N} > -\delta$ for all $t > T_\delta$, $Re \in \mathcal{R}_{Re} = [Re_m, Re_M]$, $\beta \in \mathcal{R}_\beta = [\beta_m, \beta_M]$.*

We propose the application of the resulting robust output regulator to the incompressible Navier-Stokes equations. Several configurations are tested, thus allowing for the optimisation of the closed-loop performance. In particular, we aim to identify an optimal configuration $\{\bar{x}_a, \bar{x}_s, \mathrm{y}^*\}$, for which assumption 1 holds. Here: denotes the number of actuators; $\bar{x}_a$ and $\bar{x}_s$ denote the position of the actuator and sensor, with respect to the chord length, respectively.

3 FLOW MODEL

Let Ω be an open bounded domain in $\mathbb{R}^2$ and let $T > 0$ denote the final time. The flow of an incompressible viscous Newtonian fluid can be described by the non-dimensionalised Navier-Stokes equations, which are derived from the conservation of mass and momentum, namely,

$$\begin{aligned} \partial_t \boldsymbol{u} &= -(\boldsymbol{u} \cdot \nabla)\boldsymbol{u} - \nabla p + \tfrac{1}{Re}\Delta \boldsymbol{u} + \boldsymbol{f} && \text{in } (0,T] \times \Omega, \\ 0 &= \nabla \cdot \boldsymbol{u} && \text{in } (0,T] \times \Omega, \end{aligned} \tag{3}$$

with initial condition

$$\boldsymbol{u}(0, \boldsymbol{x}) = \boldsymbol{u}_0(\boldsymbol{x}) \quad \text{in} \quad \Omega, \tag{4}$$

and boundary conditions

$$\begin{aligned} \boldsymbol{u}(t, \boldsymbol{x}) &= \boldsymbol{g}(\boldsymbol{x}) && \text{on } \Gamma_{\text{in}}, \\ \boldsymbol{u}(t, \boldsymbol{x}) &= 0 && \text{on } \Gamma_0, \\ \left(\tfrac{1}{Re}\nabla \boldsymbol{u} - pI\right)\boldsymbol{n} &= 0 && \text{on } \Gamma_{\text{out}}. \end{aligned} \tag{5}$$

Here: $\boldsymbol{x} \in \Omega$; $\boldsymbol{n}$ denotes the unit outward normal vector on $\partial\Omega = \Gamma_{\text{in}} \cup \Gamma_0 \cup \Gamma_{\text{out}}$; Γ_{in}, Γ_{out} and Γ_0 denote the inflow, outflow and wall boundaries, respectively; $\boldsymbol{u} : [0,T] \times \Omega \to \mathbb{R}^2$ is the velocity vector; $p : [0,T] \times \Omega \to \mathbb{R}$ is the pressure; $I \in \mathbb{R}^{2\times 2}$ is the identity matrix; $Re = \rho U_\infty c/\mu$ is the Reynolds number; U_∞ is the free-stream velocity (in m/s); ρ is the fluid density (in kg/m^3); $c =$ 0.1m is the chord length; $\boldsymbol{f} : [0,T] \times \Omega \to \mathbb{R}^2$ is the total body force vector field, which depends the control inputs. The latter can be expressed as $\boldsymbol{f}(t, \boldsymbol{x}) = c/\rho U_\infty^2 (f_x(t, \boldsymbol{x}), f_y(t, \boldsymbol{x}))$where f_x, f_y are the streamwise and normal component (in N/m^3). All the above listed functions are assumed to be sufficiently smooth. The wall-tangential velocity, evaluated at the selected sensor location $\boldsymbol{x}_s$,

$$\mathrm{y}(t) = u_\tau(t, \boldsymbol{x}_s) = \boldsymbol{\tau}(\boldsymbol{x}_s) \cdot \boldsymbol{u}(t, \boldsymbol{x}_s), \tag{6}$$

where $\boldsymbol{\tau}$ denotes the tangent unit vector, is chosen as the measured output. Several models for the DBD actuator force have been proposed (see, for instance, [6] for a detailed review). Here, we select a modified version of the recent model proposed by [18], which demonstrated good agreement with the experimental data. The model is characterised by an exponential dependence on the spatial coordinates and, in particular, the force is modelled by a Rayleigh distribution [see 18]; thereby,

$$\boldsymbol{f}(t,\boldsymbol{x}) = f_\tau(t,x_\tau,y_n)\boldsymbol{\tau}(\boldsymbol{x}) + f_n(t,x_\tau,y_n)\boldsymbol{n}(\boldsymbol{x}) = I(t)\frac{\lambda_f x_\tau}{(\sigma_f)^2} e^{-{x_\tau}^2/\left(2{\sigma_f}^2-\lambda_f y_n\right)}\boldsymbol{\tau}(\boldsymbol{x}), \tag{7}$$

where: $I(t) = k_v \mathrm{V}(t)/\mathrm{V}_m$ ($k_v \in \mathbb{R}$, $\mathrm{V}_m = 1$ kV) is the total plasma force; $\mathrm{V}(t) : \mathbb{R} \to \mathbb{R}$ is the amplitude variation of the operation voltage (in kV); $\mathrm{v}(t) = \mathrm{V}(t)/\mathrm{V}_m$ is the corresponding non-dimensionalised voltage input, scaled by V_m; f_τ, f_n (in $\mathrm{N/m^3}$) are the tangential and normal components, with respect to the aerofoil, of the force density , respectively; $x_\tau, y_n \geq 0$ are related to $\boldsymbol{x} = (x, y)$ by a coordinate transformation and respectively refer to the tangent and normal components, relative to the geometry, in the reference frame centred in $\boldsymbol{x}_a$.The parameters $\lambda_f = 1.6$, $\sigma_f = 1.9$, $k_v = 5200e^{1/2}\sigma_f/\lambda_f$, are chosen as in [18], where this model has been compared with particle image velocimetry (PIV) data, whilst, for sake of simplicity, a simple linear dependence of the body force on the applied peak-to-peak voltage is assumed here. System (3), (5), (4), (6), is discretised using χnavis, a general-purpose, second order, finite volume, multi-block, unsteady Reynolds averaged Navier-Stokes equations (uRaNSe) based solver, developed at CNR-INSEAN. For the sake of conciseness, details of the numerical solver are not given here, the interested reader is addressed to [2, 8].

4 FEEDBACK CONTROL PROBLEM

Consider an unknown stable linear system of the form:

$$\begin{cases} \dot{\xi} &= A\xi + B\mathrm{v}, \quad \xi(0) = \xi_0, \\ \mathrm{y} &= C\xi. \end{cases} \tag{8}$$

System (8) might be seen as a linear approximation of the spatially-discretised Navier-Stokes equations (3), (5), (4), (6), which can be obtained, for instance, using spectral decomposition methods (see [15] for linear models of fluid systems based on the Koopman operator). Although system (8) cannot represent an accurate approximation of the actual nonlinear dynamics, we aim to show how a simple robust control algorithm based on an integral action, is sufficient to effectively suppress the separation bubble along the aerofoil using real-time velocity measurements at discrete locations.

Let $P(s) = C(sI - A)^{-1}B$, whose poles have all negative real part, be the open-loop transfer function of system (8). Denoting $\tilde{\xi} = \xi - \xi^*$ and $\eta = -\mathrm{v}^*$, where ξ^* and v^* denote the references for the state and control input, respectively, the error dynamics are given by

$$\begin{cases} \dot{\tilde{\xi}} &= A\tilde{\xi} + B(\mathrm{v} + \eta), \\ \dot{\eta} &= 0, \quad \eta(0) = \eta_0, \\ \tilde{\mathrm{y}} &= C\tilde{\xi}, \end{cases} \tag{9}$$

so that the control problem can be formulated as a disturbance rejection problem, where the reference input $\mathrm{v}^* = -\eta$ can be viewed as a scalar disturbance, which matches the control input v [see 11].

Similarly to [10], the control problem becomes to design a suitable feedback law $\mathrm{v}(t)$ for system (8), based on the real-time measurement $\mathrm{y}(t)$, in order to robustly regulate the latter to a given reference region (*e.g.* $\mathrm{y}(t) \geq \epsilon > 0$). The key objective is to design v such that the closed-loop trajectories of system (8) are guaranteed to evolve within some "safe" invariant set in different scenarios, depending on uncertain parameters (*e.g.*, the Reynolds number Re and angle of attack β). Therefore, on the basis of the recent results in [11], we design a robust output regulator guaranteeing exponential convergence of the regulation error: it only requires the system to have a non-zero steady-state gain of known sign.

4.1 Control algorithm

We translate the initial control objective (2) into the following: $\mathrm{y}(t) \in \Omega_\epsilon = [\epsilon_m, \epsilon_M]$, where ϵ_m and ϵ_M are chosen positive constants. In particular, the lower bound for the output reference can be chosen in order to guarantee any a priori fixed requirement, such as, in the present application, the suppression of the separation bubble over the aerofoil; the upper bound can be chosen in order to limit the power consumption. Therefore, the control problem (similarly to [10]) becomes to design v such that the chosen controlled output y belongs to a "safe" compact set $\Omega_\epsilon = \Omega_{\epsilon_1} \times \Omega_{\epsilon_2} \times ... \times \Omega_{\epsilon_{n_p}}$. To this aim, the reference output y^* is chosen as

$$\mathrm{y}^*(t) = \begin{cases} \epsilon_m, & \text{if } \mathrm{y}(t) < \epsilon_m, \\ \mathrm{y}(t), & \text{if } \mathrm{y}(t) \in \Omega_\epsilon, \\ \epsilon_M, & \text{if } \mathrm{y}(t) > \epsilon_M. \end{cases} \tag{10}$$

The resulting control algorithm reads

$$\begin{cases} \dot{\hat{\eta}} & = k \ \mathrm{sign}(P(0))\tilde{\mathrm{y}}, \quad \hat{\eta}(0) = \hat{\eta}_0, \\ \mathrm{v} & = -\hat{\eta}. \end{cases} \tag{11}$$

The overall control algorithm (11), (10) depends on: the measured outputs y; the bounded references y^*; the known sign of $P(0)$; the positive design parameters k, ϵ_m, ϵ_M. Note that, when $\epsilon = \epsilon_m = \epsilon_M$ the control algorithm (11), (10) reduces to an output regulator with a constant output reference.

4.2 Stability Analysis

The stability properties of the closed-loop system are summarised by the following theorem.

Theorem 1. *Consider the closed-loop system (8), (11), (10). Assume that $P(0) \neq 0$ with known sign. Then, for any initial condition $(\xi_0, \eta_0, \hat{\eta}_0)$, there exist sufficiently small $k^* > 0$, such that the regulation error $\tilde{y} = y(t) - y^*(t)$ and the control input error $v(t) - v^*(t)$ exponentially tend to zero, as t tends to infinity, for any $0 < k \leq k^*$.*

Proof. a). Case $\epsilon = \epsilon_m = \epsilon_M$. System (9) can be rewritten as

$$\tilde{\mathrm{Y}}(s) = P(s)\left(\mathrm{v}(s) + \eta\right), \quad P(s) \doteq \frac{n_P(s)}{d_P(s)}. \tag{12}$$

The stability of the closed-loop system is determined by the zeros of the transfer function

$$Q(s) = 1 + kP(s)\left(\frac{\text{sign}(P(0))}{s}\right) \doteq \frac{n_Q(s)}{d_Q(s)}. \tag{13}$$

By the root locus, for sufficiently small $k > 0$, r zeros of $Q(s)$ are sufficiently close to the r poles of $P(s)$ and, therefore, they have negative real part. The remaining branch of the root locus starts from 0 in the s-plane with angle π, so that also the remaining zeros of $Q(s)$ have negative real part.
b). Case $\epsilon_m < \epsilon_M$. Let $\tilde{\eta} = \mathrm{v} - \mathrm{v}^* = \eta - \hat{\eta}$ and $\tilde{\chi} = [\tilde{\xi}, \tilde{\eta}]^{\mathrm{T}}$. The closed-loop error dynamics can be written as

$$\begin{aligned}\dot{\tilde{\chi}} &= \begin{bmatrix} A & B \\ -k\ \text{sign}(P(0))C & 0 \end{bmatrix}\tilde{\chi} \doteq A_c\tilde{\chi},\\ \tilde{\mathrm{y}} &= [C, 0]\,\tilde{\chi}.\end{aligned}$$

The characteristic polynomial of the closed-loop matrix A_c can be computed as $p_{A_c}(s) = \det(sI_{r+1} - A_c) = sd_P(s) + kn_P(s)\text{sign}(P(0)) = n_Q(s)$. Therefore, A_c is Hurwitz, as its eigenvalues coincide with roots of $n_Q(s)$ and have negative real part for any sufficiently small k. Thus, there exist two symmetric, positive definite matrices $\mathcal{P}$ and $\mathcal{Q}$ satisfying the Lyapunov equation: $\mathcal{P}A_c + A_c^{\mathrm{T}}\mathcal{P} = -\mathcal{Q}$. $\mathcal{V}(t) \doteq \tilde{\chi}^{\mathrm{T}}(t)\mathcal{P}\tilde{\chi}(t)$, satisfying

$$\alpha_1\|\tilde{\chi}(t)\|^2 \leq \mathcal{V}(t) \leq \alpha_2\|\tilde{\chi}(t)\|^2, \tag{14}$$

where $\alpha_1,\ \alpha_2 > 0$ are positive constants. The time derivative of $\mathcal{V}(t)$, along the trajectories of the closed-loop system satisfies the following inequality: $\dot{\mathcal{V}} \leq -\tilde{\chi}^{\mathrm{T}}\mathcal{Q}\tilde{\chi} + 2\tilde{\chi}^{\mathrm{T}}\mathcal{P}\zeta(\tilde{\chi}) \leq -\mathcal{M}\|\tilde{\chi}\|^2 \leq -\mathcal{M}\|\tilde{\chi}\|^2$,where $\mathcal{M} = \|\mathcal{Q}\|$. Therefore, there exists an $\alpha_3 > 0$ such that

$$\dot{\mathcal{V}} \leq -\alpha_3\|\tilde{\chi}\|^2 \leq -\frac{\alpha_3}{\alpha_2}\mathcal{V}, \tag{15}$$

thus implying the closed-loop boundedness and the exponential convergence to zero of both the regulation error $\tilde{\mathrm{y}}(t)$ and the control input error $\mathrm{v}(t) - \mathrm{v}^*$, as t tends to infinity. Let $\tilde{\xi} = \xi - \xi^*$ and $\tilde{\eta} = \mathrm{v} - \mathrm{v}^*$. When the output vector belongs to the compact set Ω_ϵ, we have: $\tilde{\xi} \equiv 0$, $\dot{\tilde{\xi}} \equiv 0$, $\dot{\tilde{\eta}} \equiv 0$. Thus, for any $t \geq 0$ such that $\mathrm{y}(t) \in \Omega_\epsilon$, $\dot{\mathcal{V}}(t) \equiv 0$. When the output does not belong to the reference region, there exist three positive constants $\alpha_1,\ \alpha_2,\ \alpha_3 > 0$ such that $\mathcal{V}(t)$ and its time derivative satisfy (14) and (15), respectively. Therefore, for any $t \geq 0$ such that $\mathrm{y}(t) \notin \Omega_\epsilon$, $\dot{\mathcal{V}}(t) < 0$ and the distance $\mathrm{d}_{\mathcal{P}}(\chi(t), \Omega_\chi) \doteq \inf_{\bar{\chi}\in\Omega_\chi}\|\chi - \bar{\chi}\|_{\mathcal{P}} \doteq \sqrt{\tilde{\chi}^{\mathrm{T}}\mathcal{P}\tilde{\chi}}$,between χ and its reference set Ω_χ satisfies $\mathrm{d}^2_{\mathcal{P}}(\chi(t), \Omega_\chi) \leq \alpha_2\|\tilde{\chi}\|^2 \leq e^{-\alpha t}\delta$,where $\alpha = \alpha_3/\alpha_2$ and $\delta = \mathcal{V}(0)\alpha_2/\alpha_1$. Since $0 \leq \mathcal{V}(t) \in \mathcal{C}^1$ is lower bounded and its derivative is semi-negative definite, it admits a finite limit [see 7, p. 61]. Closed-loop boundedness and exponential convergence of $\dot{\mathcal{V}}(t)$ (and, therefore, of $\tilde{\xi}$ and $\dot{\tilde{\eta}}$) to zero are thus guaranteed, according to Barbalats lemma, as $\mathcal{V}(t)$ is uniformly continuous. Consequently, $\xi(t)$ converges to a constant reference $\bar{\xi} \in \Omega_\xi$ and $\mathrm{v}(t)$ converges to a constant value $\bar{\mathrm{v}}$, as t tends to infinity. If $\bar{\mathrm{v}} \notin \Omega_\eta$, then $\bar{\mathrm{y}} = C\bar{\xi} = -P(0)\bar{\mathrm{v}} \notin \Omega_\epsilon$, which contradicts $\bar{\xi} \in \Omega_\xi$. Therefore, $\bar{\mathrm{v}} \in \Omega_\eta$ and the distance $\mathrm{d}_{\mathcal{P}}(\chi(t), \Omega_\chi)$ exponentially tends to zero, as t tends to infinity. □

5 OPTIMIZATION METHOD

The MODPSO algorithm is used here for the minimization of the time-averaged input signal and the drag-to-lift ratio, $\boldsymbol{\phi} \doteq \{\langle \mathrm{v} \rangle, C_D/C_L\}^T$, versus the optimization variables, $\boldsymbol{\theta} \doteq \{\Delta_s, \epsilon_m\}^T \in \mathcal{D}$. Here: $\langle \cdot \rangle$ denotes the time-average; $\Delta_s \doteq |\bar{x}_a - \bar{x}_s|$ is the distance between the sensor and the actuator, with respect to the chord length; $(\cdot)^{\mathrm{T}}$ denotes the transpose of $(\cdot)$. The original PSO algorithm was introduced in [9], based on the social-behavior metaphor of a swarm of bees searching for food and belongs to the class of metaheuristic algorithms for single-objective derivative-free global optimization. Pinto et al. [13] proposed a multi-objective deterministic extension of the method as

$$\begin{cases} \boldsymbol{v}_i^{k+1} = \gamma \left[\boldsymbol{v}_i^k + c_1 \left(\mathbf{p}_i - \boldsymbol{\theta}_i^k \right) + c_2 \left(\mathbf{g}_i - \boldsymbol{\theta}_i^k \right) \right] \\ \boldsymbol{\theta}_i^{k+1} = \boldsymbol{\theta}_i^k + \boldsymbol{v}_i^{k+1} \end{cases} \tag{16}$$

where $\boldsymbol{v}_i^k$ and $\boldsymbol{\theta}_i^k$ are the velocity and the position of the i-th particle at the k-th iteration, γ is a constriction factor, c_1 and c_2 are the cognitive and social learning rate, and $\mathbf{p}_i$ and $\mathbf{g}_i$ are the cognitive and social attractor.

The algorithm formulation and setup is defined as suggested in [12]: the cognitive attractor $\mathbf{p}_i$ is the personal minimizer of the aggregate function $\Phi(\boldsymbol{\theta}_i) = \sum_{m=1}^{M} w_m \phi_m(\boldsymbol{\theta}_i)$, where $w_m = 1/M$ $(\forall m)$ is the weight associated to the m-th objective function with M the number of objective functions; the social attractor $\mathbf{g}_i$ is the closest point to the i-th particle of the Pareto front; the number of particles is set equal to 32, initialized over the domain $\mathcal{D}$ its boundary with a Hammersley distribution and non-null velocity [3]; the coefficients correspond to $\gamma = 0.721$, $c_1 = c_2 = 1.655$ [5]; a semi-elastic wall-type approach [17] is used to keep the particles within $\mathcal{D}$. The number of iterations is set to 1000.

6 RESULTS

Although the resulting robust control algorithm is designed on the basis of an unknown theoretical linear model, we propose its application to the flow separation control problem, along a NACA0012 profile, which is of practical interest. We only assume, coherently with assumption 1, a positive steady-state gain for any actuator/sensor pair.

6.1 Simulations

The computational grid has $N = 127,872$ total volumes and is divided into extremely fine actuator grids (see figure 1 right), a fine C-type inner grid (see figure 1 left) and coarser outer grids. The connections between the different grids are handled using an overlapping grid approach. The inner region around the profile has 320×96 volumes, in the tangent and normal direction, respectively; the points are clustered towards the wall, where the mesh spacing is equal to 2.1×10^{-4}. In the near wake region, 128×192 volumes, in the streamwise and vertical direction, respectively, are clustered around the wake of the profile.

The performance of the proposed control scheme (10), (11), is tested for the flow past a NACA0012 profile at $Re = 20,000$, in 21 different configurations: the actuator is placed at $\bar{x}_a = 0.02$, as preliminary tests (which are not reported here for the sake of brevity) showed a deterioration in the performance when it is moved further downstream; the distance Δ_s between

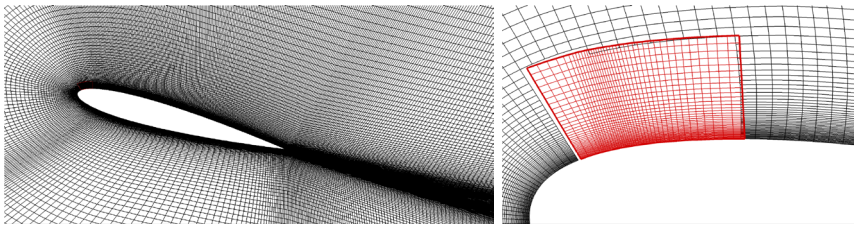

Figure 1: Computational grid around the NACA0012 profile (left) and actuator's block (right).

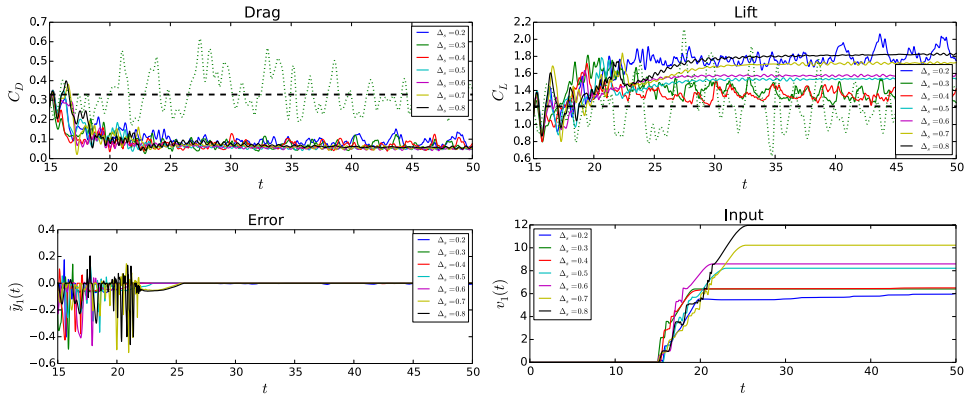

Figure 2: Simulation results in the scenario $\epsilon_m = 0.05$.

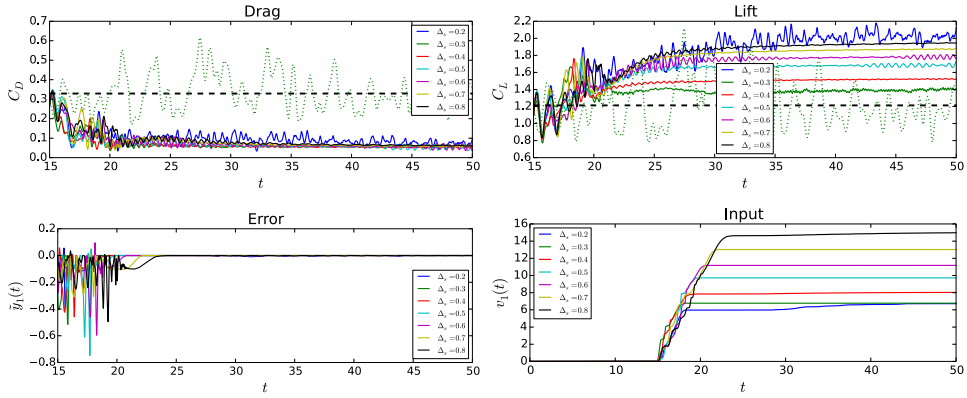

Figure 3: Simulation results in the scenario $\epsilon_m = 0.1$.

the sensor and the actuator is varied between 0.3 and 0.8; three different lower bounds $\epsilon_m = 0.05$, $\epsilon_m = 0.1$, $\epsilon_m = 0.2$ of the reference set Ω_ϵ are considered, while the upper bound is $\epsilon_M = \epsilon_m + 0.05$. The corresponding results are shown in figures 2-5. The controller is activated between $t_0 = 15$ and $t_f = T = 50$. The angle of attack is $\beta_0 = 15°$. The output measurements $\mathrm{y}(t) = u_{\boldsymbol{\tau}}(t, x_s, y_s)$ are taken at $y_n = 0.0005$ above the aerofoil. The chosen control gain is $k = 20$.

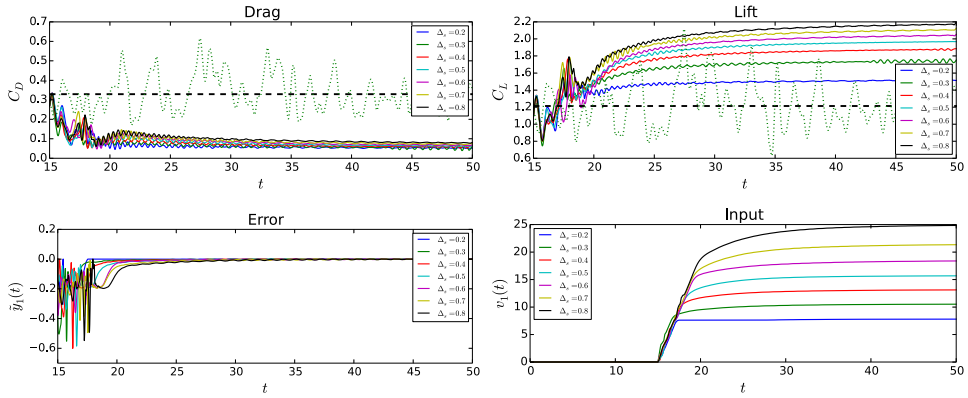

Figure 4: Simulation results in the scenario $\epsilon_m = 0.2$.

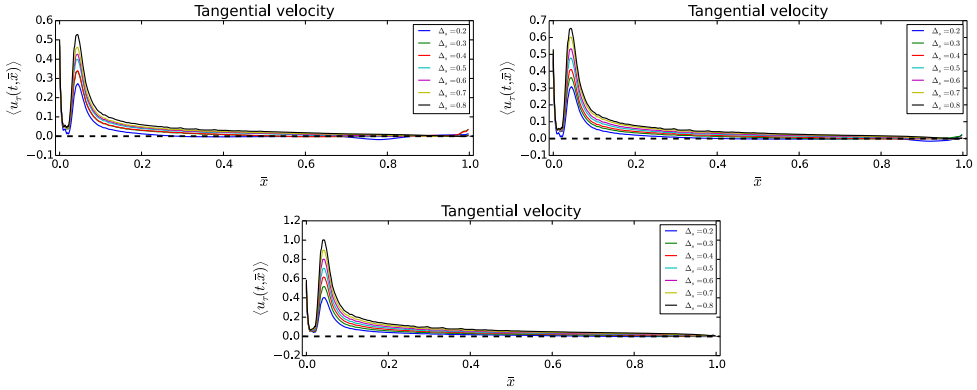

Figure 5: Time-averaged tangential velocity for $\epsilon_m = 0.005$ (top left), $\epsilon_m = 0.01$ (top right) and $\epsilon_m = 0.02$ (bottom).

6.2 Optimization

The Pareto front of the non dominated solutions obtained by MODPSO is shown in Fig. 6 (a). The associated configurations in the Δ_s-ϵ_m plane are shown in Figs. 6 (b) and (c) versus $\langle \mathrm{v} \rangle$ and C_D/C_L, respectively. Three sub-sets are identified based on the clustering in the Δ_s-ϵ_m plane. The clustering reflects clearly on the $\langle \mathrm{v} \rangle$-$C_D/C_L$ trade-off. For each set, one solution is selected for further analysis. Specifically, solution 1 corresponds to $\Delta_s = 0.4$ and $\epsilon_m = 0.1$, providing a quite balanced compromise between $\langle \mathrm{v} \rangle$ and C_D/C_L. Solution 2 has $\Delta_s = 0.3$ and $\epsilon_m = 0.2$ and one of the lowest values for C_D/C_L, whereas solution 3 corresponds to $\Delta_s = 0.2$ and $\epsilon_m = 0.1$ with a quite low value of $\langle \mathrm{v} \rangle$.

The instantaneous vorticity contours for the selected solutions, are shown in figure 7; 101 non-dimensional vorticity levels over the range $[-15, 15]$, results for both with and without the actuation are reported for comparison purposes. Without the actuation, strong vortex structures are generated as a consequence of both the strong adverse pressure gradients and the boundary layer separation, which occurs on the upper side of the profile. The proposed control algorithm

significantly reduces the boundary layer separation and avoids the generation of large vortical structures.

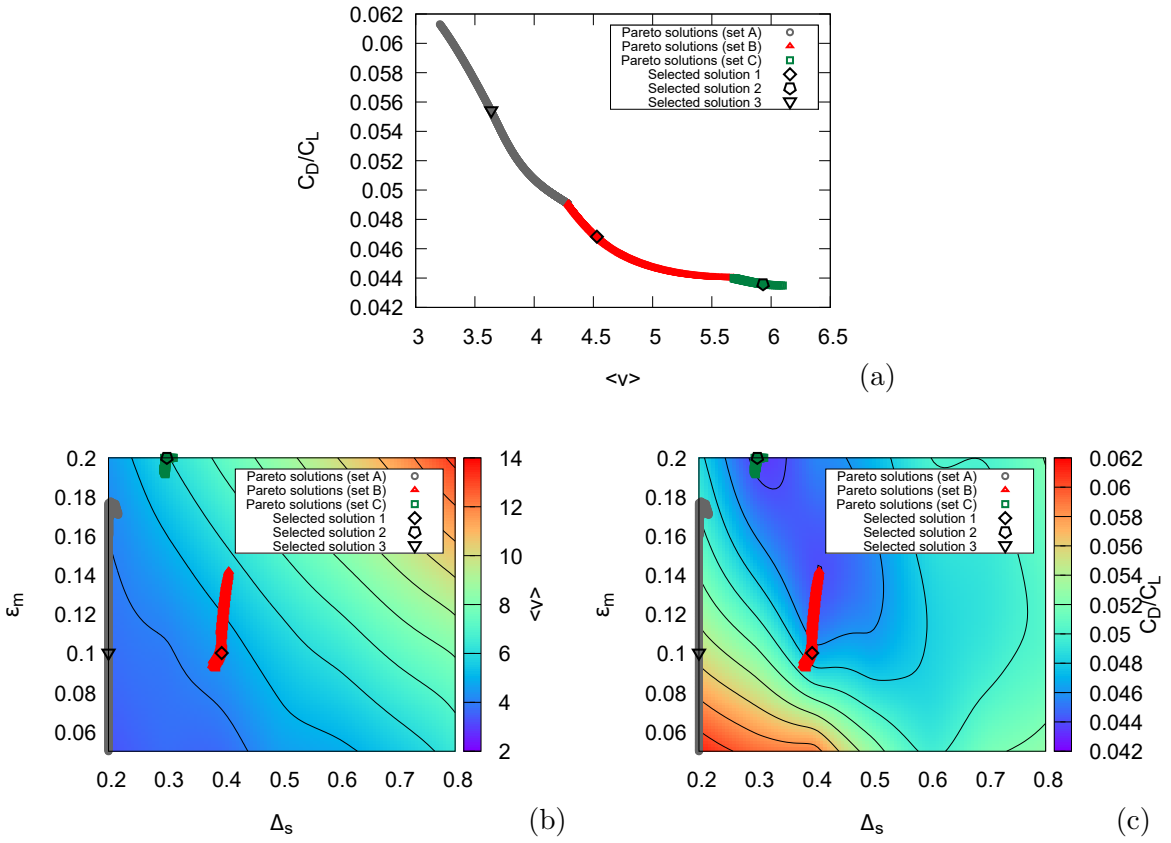

Figure 6: Pareto front obtained by MODPSO (a), $\langle v \rangle$ (b), and C_D/C_L (c) versus Δ_s and ϵ_m showing Pareto sub-sets and selected solutions

7 CONCLUSIONS

We addressed the practical problem of robustly controlling the unsteady flow separation over an aerofoil, using the plasma actuator's voltage as the control input and realistically available real-time velocity measurements as the control output. In particular, we formulated the flow separation problem as a simple output regulation problem and solved the latter by designing a robust feedback control algorithm. Accurate numerical simulations of flows past a NACA0012 at Reynolds $Re = 20,000$ and angle of attack $\beta = 15°$ are performed in order to both test the control effectiveness and optimize the performance of the closed-loop system. Although the proposed controller is simple, as it is based on an integral action, it is able to effectively suppress the separation bubble, as well as the shedding vortices. Different configurations were tested, to the aim of identifying optimal positions of the actuator/sensor pairs along the aerofoil and the corresponding references for the available real-time velocity measurements. Finally, a multi-

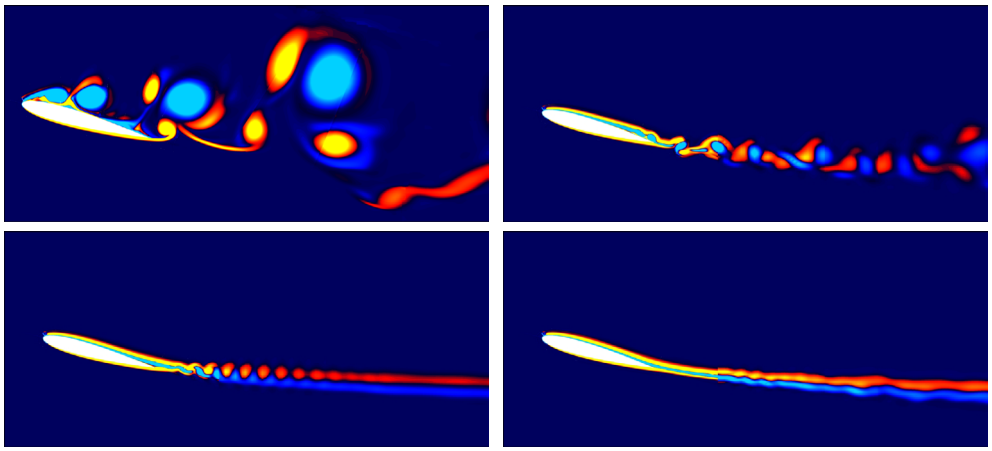

Figure 7: Vorticity contours using 101 levels over the range $[-15, 15]$: without control (top left), solutions 1 (top right), 2 (bottom left) and 3 (bottom right).

objective deterministic particle swarm optimization algorithm was applied to identify the Pareto set of non dominated configurations considering as objectives the time-averaged input signal and the drag-to-lift ratio. Three sub-sets of non dominated configurations were identified based on the solution clustering and, for each set, one solution was selected for further investigations and demonstration of the methodology.

8 ACKNOWLEDGEMENTS

The research leading to these results has received fundings from: the People Programme (Marie Curie Actions) of the European Unions Seventh Framework Programme (FP7/2007-2013) under REA grant agreement no 608322; the present work was also supported by the Project RESMARE (Ricerca E Servizi per il MARE) funded by the Lazio Region.

References

[1] N. Benard and E. Moreau. Plasma flow control - autonomous lift improvement by slope-seeking. *AIAA paper*, 2009:4182, 2009.

[2] R. Broglia, S. Zaghi, R. Muscari, and F. Salvadore. Enabling hydrodynamics solver for efficient parallel simulations. In *Proceedings International Conference on High Performance Computing & Simulation (HPCS)*, pages 803–810, Bologna, Italy, 2014.

[3] X. Chen, M. Diez, M. Kandasamy, Z. Zhang, E.F. Campana, and F. Stern. High-fidelity global optimization of shape design by dimensionality reduction, metamodels and deterministic particle swarm. *Engineering Optimization*, 47(4):473–494, 2015.

[4] Y. C. Cho and W. Shyy. Adaptive flow control of low-reynolds number aerodynamics using dielectric barrier discharge actuator. *Progress in Aerospace Sciences*, 47:495–521, 2011.

[5] M. Clerc. Stagnation analysis in particle swarm optimization or what happens when nothing happens. *Online at http://clerc. maurice. free. fr/pso*, 2006.

[6] T. C. Corke, C. L. Enloe, and S. P. Wilkinson. SDBD plasma enhanced aerodynamics: concepts, optimization and applications. *Progress in Aerospace Sciences*, 43:193–217, 2007.

[7] R. Courant. *Differential and Integral Calculus*, volume I. Blackie and Son, 1937.

[8] A. Di Mascio, R. Broglia, and R. Muscari. Prediction of hydrodynamic coefficients of ship hulls by high-order Godunov-type methods. *J. Marine Sci. Tech.*, 14:19–29, 2009.

[9] J. Kennedy and R. Eberhart. Particle swarm optimization. In *Proceedings of the IEEE International Conference on Neural Networks*, volume 4, pages 1942–1948, 1995.

[10] R. Marino, L. Pasquale, S. Scalzi, and C. M. Verrelli. Automatic rotor speed reference generator for electric vehicles under slip constraints. *IEEE Trans. on Intelligent Transportation Systems*, 16(6):3473–3478, 2015.

[11] R. Marino and P. Tomei. Output regulation for unknown stable linear systems. *Automatica*, 60(8):2213–2218, 2015.

[12] R Pellegrini, E F Campana, M Diez, A Serani, F Rinaldi, G Fasano, U Iemma, G Liuzzi, S Lucidi, and F Stern. Application of derivative-free multi-objective algorithms to reliability-based robust design optimization of a high-speed catamaran in real ocean environment. In *Engineering Optimization IV - Rodrigues et al. (Eds.)*, 2014.

[13] A. Pinto, D. Peri, and E. F. Campana. Multiobjective optimization of a containership using deterministic particle swarm optimization. *Journal of Ship Research*, 51(3):217–228, 2007.

[14] M. Riherd and S. Roy. Serpentine geometry plasma actuators for flow control. *J. Appl. Phys.*, 114:083303, 2013.

[15] C. W. Rowley, I. Mezi/'c, S. Bagheri, P. Schlatter, and D. S. Henningson. Spectral analysis of nonlinear flows. *J. Fluid Mech.*, 641:115–127, 2009.

[16] T. Segawa, J. Pang, T. Ikehara, R. Maeda, and H. Yoshida. MEMS-based cantilever sensor for fluid dynamics measurements. *Research Signpost ISBN: 978-81-308-0220-6*, pages 217–243, 2010.

[17] A. Serani, C. Leotardi, U. Iemma, E.F. Campana, G. Fasano, and M. Diez. Parameter selection in synchronous and asynchronous deterministic particle swarm optimization for ship hydrodynamics problems. *Applied Soft Computing*, 49:313 – 334, 2016.

[18] Q. Yang and Y. M. Chung. Numerical study of reducing turbulent skin-friction drag using DBD plasma actuators. *EDRFCM 2015, Cambridge*, 2015.